Diffusion behavior in Nickel–Aluminum and Aluminum–Uranium diluted alloys

CrossMark

Viviana P. Ramunni *

CONICET, Avda. Rivadavia 1917, Cdad. de Buenos Aires C.P. 1033, Argentina
Departamento de Materiales, CAC-CNEA, Avda. General Paz 1499, 1650 San Martín, Argentina

ABSTRACT

Impurity diffusion coefficients are entirely obtained from a low cost classical molecular statics technique (CMST). In particular, we show how CMST is appropriate in order to describe the impurity diffusion behavior mediated by a vacancy mechanism. In the context of the five-frequency model, CMST allows to calculate all the microscopic parameters, namely: the free energy of vacancy formation, the vacancy-solute binding energy and the involved jump frequencies, from them, we obtain the macroscopic transport magnitudes such as: correlation factor, solvent-enhancement factor, Onsager and diffusion coefficients. Specifically, we perform our calculations in f.c.c. diluted Ni–Al and Al–U alloys. Results for the tracer diffusion coefficients of solvent and solute species are in agreement with available experimental data for both systems. We conclude that in Ni–Al and Al–U systems solute atoms migrate by direct interchange with vacancies in all the temperature range where there are available experimental data. In the Al–U case, a vacancy drag mechanism could occur at temperatures below 550 K.

1. Introduction

The low enrichment of U–Mo alloy dispersed in an Al matrix is a prototype for new experimental nuclear fuels [1]. When these metals are brought into contact, diffusion in the Al/U—Mo interface gives rise to interaction phases. Also, when subjected to temperature and neutron radiation, phase transformation from γU to αU occurs and intermetallic phases develop in the U–Mo/Al interaction zone. Fission gas pores nucleate in these new phases during service producing swelling and deteriorating the alloy properties [1,2]. An important technological goal is to delay or directly avoid undesirable phase formation by inhibiting interdiffusion of Al and U components. Some of these compounds are believed to be responsible for degradation of properties [3].

Housseau et al. [4], based on the effective diffusion coefficients values calculated from their experimental permeation tests, have demonstrated that these undesirable phases have not influence on the mobility of U in Al. On the other hand, Bierlin and Green [5] have reported the activation energy values of U mobility in Al, based on the maximum rate of penetration of U into Al.

On the other hand, Brossa et al. [6], have produced couples and triplets structures using deposition methods to study the efficient diffusion barriers that should have simultaneously, a good bonding effect and a good thermal conductivity. The practical interest of a Ni barrier is shown by several publications concerning with the diffusion in the systems Al—Ni, Ni—U and Al—Ni—U. The study of the Ni—Al binary system was, limited to solid samples of the sandwich-type, clamped together by a titanium screw and diffusion treatments have been carried out. Results from this work [6], have inspired present calculations.

Therefore it is important to study carefully and with special attention the initial microscopic processes that originate these intermetallic phases. In order to deal with this problem we started studying numerically the static and dynamic properties of vacancies and interstitials defects in the Al(U) bulk and in the neighborhood of a $(111)Al/(001)\alpha U$ interface using molecular dynamics calculations [7,8]. Here, we review our previous works [7,8], performing calculation of the tracer diffusion coefficients in binary Ni–Al and Al–U alloys, using analytical expressions of the diffusion parameters in terms of microscopical magnitudes.

We have summarized the theoretical tools needed to express the diffusion coefficients in terms of microscopic magnitudes such as, the jump frequencies, the free vacancy formation energy and the vacancy-solute binding energy. Then we start with non-equilibrium thermodynamics in order to relate the diffusion coefficients with the phenomenological Onsager L-coefficients. The microscopic kinetic theory, allows us to write the Onsager

* Address: CONICET, Avda. Rivadavia 1917, Cdad. de Buenos Aires C.P. 1033, Argentina. Tel.: +54 11 6772 7298; fax: +54 11 6772 7303.
E-mail address: vpram@cnea.gov.ar

coefficients in term of the jump frequency rates [9,10], which are evaluated from the migration barriers and the phonon frequencies under the harmonic approximation. The lattice vibrations are treated within the conventional framework of Vineyard [11] that corresponds to the classical limit.

The jump frequencies are identified by the model developed further by Le Claire in Ref. [12], known as the five-frequency model for f.c.c lattices. The method includes the jump frequency associated with the migration of the host atom in the presence of an impurity at a first nearest neighbor position. All this concepts need to be put together in order to correctly describe the diffusion mechanism. Hence, in the context of the shell approximation, we follow the technique developed by Allnatt in Refs. [9,10] to obtain the corresponding transport coefficients, which are related to the diffusion coefficients through the flux equations.

A similar procedure for f.c.c. structures was performed by Mantina et al. [13,14] for Mg, Si and Cu diluted in Al but using density functional theory (DFT). Also, using DFT calculations for b.c.c. structures, Choudhury et al. [15] have calculated the tracer self-diffusion and solute diffusion coefficients in diluted $Fe-Ni$ and $Fe-Cr$ alloys including an extensive analysis of the Onsager L-coefficients.

In the present work, we do not employ DFT, instead we use a classical molecular statics technique coupled to the Monomer method [16]. This much less computationally expensive method allows us to compute at low cost a bunch of jump frequencies from which we can perform averages in order to obtain more accurate effective frequencies. Although we use classical methods, we have also reproduced the migration barriers for $Ni-Al$ with DFT calculations coupled to the Monomer method [17].

We proceed as follows, first of all we validate the five-frequency model using the $Ni-Al$ system as a reference case for which there is a large amount of experimental data and numerical calculations [18]. Since, the $Al-U$ and $Ni-Al$ systems share the same crystallographic f.c.c. structure, the presented description is analogous for both alloys. The full set of frequencies are evaluated employing the economic Monomer method [16]. The Monomer is used to compute the saddle points configurations from which we obtain the jumps frequencies defined in the five-frequency model.

For the $Ni-Al$ system case, our results of the tracer solute and self-diffusion coefficients are in good agreement with the experimental data. In this case we found that Al in Ni, at diluted concentrations, migrates as a free specie in the full range of temperatures here considered. In the case of $Al-U$, present calculations show that both, the tracer and self-diffusion coefficients agree very well with the available experimental data in Ref. [4], although a vacancy drag mechanism could occur at temperatures below 500 K, while, for at high temperatures the solute U migrates by direct interchange with the vacancy.

The paper is organized as follows: In Section 2 we briefly introduce a summary of the macroscopic equations of atomic transport that are provided by non-equilibrium thermodynamics [19–21]. In this way analytical expressions of the intrinsic diffusion coefficients in binary alloys in terms of Onsager coefficients are presented. Section 3, is devoted to give the way to evaluate the Onsager phenomenological coefficients following the procedure of Allnatt [9,10] in terms of the jumps frequencies in the context of the five-frequency model. In Section 4 we show the methodology used to evaluate the tracer diffusion coefficients for the solvent and solute atoms, as well as, the so called solvent enhancement factor. Finally, in Section 5 we present our numerical results using the theoretical procedure here summarized, which show a perfect accuracy with available experimental data, also we give an expression for the vacancy wind parameter which gives essential information about the flux of solute atoms induced by vacancy flow. The last section briefly presents some conclusions.

2. Theory summary: the flux equations

Isothermal atomic diffusion in binary $A-S$ alloys can be described through a linear expression between the fluxes $\boldsymbol{J}_k$ and the driving forces related by the Onsager coefficients L_{ij} as,

$$\boldsymbol{J}_k = \sum_i^N L_{ki} \boldsymbol{X}_i, \tag{1}$$

where N is the number of components in the system, $\boldsymbol{J}_k$ describes the flux vector density of component k, while $\boldsymbol{X}_k$ is the driving force acting on component k. The second range tensor L_{ij} is symmetric ($L_{ij} = L_{ji}$) and depends on pressure and temperature, but is independent of the driving forces $\boldsymbol{X}_k$. From (1) the 1st Fick's law, which describes the atomic jump process on a macroscopic scale, can be recovered. On the other hand, for each k component, the driving forces may be expressed, in absence of external force, in terms of the chemical potential μ_k, so that [19],

$$\boldsymbol{X}_k = -T \nabla \left(\frac{\mu_k}{T} \right). \tag{2}$$

In (2) T is the absolute temperature, and the chemical potential μ_k is the partial derivative of the Gibbs free energy with respect to the number of atoms of specie k that is,

$$\mu_k = \left(\frac{\partial G}{\partial N_k} \right)_{T,P,N_{j \neq k}} = \mu^\circ_k(T,P) + k_B T \ln(c_k \gamma_k), \tag{3}$$

where γ_k, is the activity coefficients, which is defined in terms of the activity $a_k = \gamma_k c_k$ and c_k, is the molar concentration of specie k.

For the particular case of a binary diluted alloy (A, S) with N available lattice sites per unit volume, containing molar concentrations c_A for host atoms, c_S of solute atoms (impurities) and c_V vacancies, the fluxes in terms of the Onsager coefficients are expressed as,

$$\boldsymbol{J}_A = -\frac{k_B T}{N} \left(\frac{L_{AA}}{c_A} - \frac{L_{AS}}{c_S} \right) \left(1 + \frac{\partial ln \gamma_A}{\partial ln c_A} \right) \nabla c_A, \tag{4}$$

$$\boldsymbol{J}_S = -\frac{k_B T}{N} \left(\frac{L_{SS}}{c_S} - \frac{L_{AS}}{c_A} \right) \left(1 + \frac{\partial ln \gamma_S}{\partial ln c_S} \right) \nabla c_S, \tag{5}$$

and

$$\boldsymbol{J}_V = -(\boldsymbol{J}_A + \boldsymbol{J}_S). \tag{6}$$

From (4) and (5), we define

$$D_A = \frac{k_B T}{N} \left(\frac{L_{AA}}{c_A} - \frac{L_{AS}}{c_S} \right) \phi_A, \tag{7}$$

$$D_S = \frac{k_B T}{N} \left(\frac{L_{SS}}{c_S} - \frac{L_{SA}}{c_A} \right) \phi_S. \tag{8}$$

In the case of $c_A, c_S \gg c_V$, the diffusion coefficient for the vacancy is given by,

$$D_V = \frac{k_B T}{c_V} (L_{AA} + L_{SS} + 2 L_{AS}). \tag{9}$$

In (7) and (8), D_A and D_S are the intrinsic diffusion coefficients for solvent A and solute S respectively, while D_V is the vacancy diffusion coefficient [22]. In (7) and (8) the quantities ϕ_A, ϕ_S are the thermodynamic factors,

$$\phi_A = \left(1 + \frac{\partial ln \gamma_A}{\partial ln c_A} \right) = \phi_S = \left(1 + \frac{\partial ln \gamma_S}{\partial ln c_S} \right). \tag{10}$$

Murch and Qin [21] have shown that the standard intrinsic diffusion coefficients in (7) and (8) can be expressed in terms of the tracer diffusion coefficients $D_A^\star, D_S^\star$ which are measurable quantities, and the collective correlation factor f_{ij} ($i, j = A, S$) as:

$$D_A = D_A^0 \left[f_{AA} - \frac{c_A}{c_S} f_{AS}^{(A)} \right] \phi_A = D_A^\star \left[\frac{f_{AA}}{f_A} - \left(\frac{c_A}{c_S} \right) \frac{f_{AS}^{(A)}}{f_A} \right] \phi_A, \qquad (11)$$

$$D_S = D_S^0 \left[f_{SS} - \frac{c_S}{c_A} f_{AS}^{(S)} \right] \phi_S = D_S^\star \left[\frac{f_{SS}}{f_S} - \left(\frac{c_S}{c_A} \right) \frac{f_{AS}^{(S)}}{f_S} \right] \phi_S. \qquad (12)$$

The intrinsic diffusion coefficients in (11) and (12) are known as the modified Darken equations, where $D_i^0 = s^2 \Gamma_i / 6$ ($i = A, S$) are the diffusion coefficients of atoms of specie i in a complete random walk performing Γ_i jumps of length s per unit time. The collective correlation factors f_{ij} are related to the L_{ij} coefficients through,

$$f_{AA} = \frac{k_B T}{N c_A} L_{AA} \left(\frac{1}{D_A^0} \right); \quad f_{SS} = \frac{k_B T}{N c_S} L_{SS} \left(\frac{1}{D_S^0} \right), \qquad (13)$$

and for the mixed terms,

$$f_{AS}^{(A)} = \frac{k_B T}{N c_A} L_{AS}^{(A)} \left(\frac{1}{D_A^0} \right); \quad f_{AS}^{(S)} = \frac{k_B T}{N c_S} L_{AS}^{(S)} \left(\frac{1}{D_S^0} \right). \qquad (14)$$

The tracer correlation factors f_A, f_S are defined as the ratios $f_A = D_A^\star / D_A^0$ and $f_S = D_S^\star / D_S^0$ respectively. The term in square brackets in the second term of Eqs. (11) and (12), is the vacancy wind factor G [24]. In the next sections, we present the Onsager coefficients in terms of the atomic jump frequencies taken from Ref. [9,10].

3. The L-coefficients in the shell approximation

In order to understand the effect of different vacancy exchange mechanisms on solute diffusion, we adopt an effective five frequency model à la Le Claire [12] for f.c.c. lattices, assuming that the perturbation of the solute movement by a vacancy V, is limited to its immediate vicinity. Fig. 1 defines the jump rates ω_i ($i = 1, 2, 3, 4$) considering only jumps between first neighbors. For them, w_2 implies in the exchange between the vacancy and the solute, w_1 when the exchange between the vacancy and the solvent atom lets the vacancy as a first neighbor to the solute (positions denoted with circled 1 in Fig. 1). The frequency of jumps such that the vacancy goes to sites that are second neighbor of the solute is denoted by ω_3 (sites with circled 2). The model includes the jump
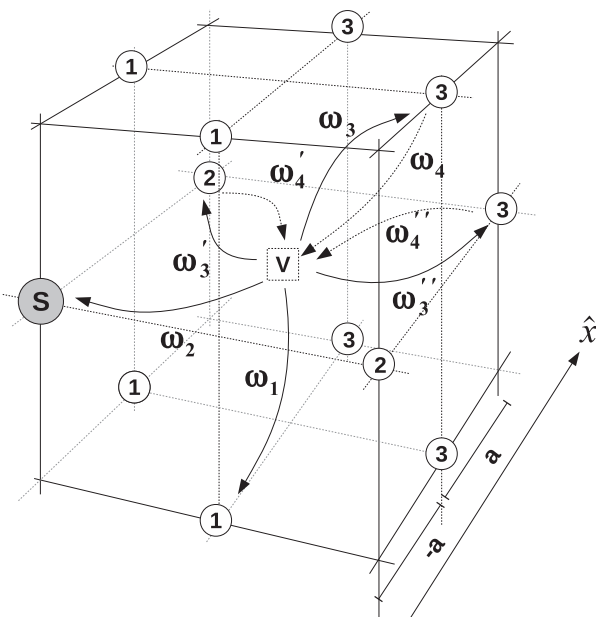
rate ω_4 for the inverse of ω_3. Jumps toward sites that are third and forth neighbor of the solute are all denoted with ω_3' and ω_3'' respectively while ω_4' and ω_4'' are used for their respective inverse frequency jumps. The jump rate ω_0 is used for vacancy jumps among sites more distant than forth neighbors of the solute atom. In this context, that enables association (ω_4) and dissociation reactions (ω_3), i.e. the formation and break-up of pairs, the model include free solute and vacancies to the population of bounded pairs. It is assumed that a vacancy which jumps from the second to the third shell, with ω_0, will never return (or returns from a random direction). As in Ref. [15] we express

$$7\omega_3^\star = 2\omega_3 + 4\omega_3' + \omega_3'', \qquad (15)$$

and

$$7\omega_4^\star = 2\omega_4 + 4\omega_4' + \omega_4''. \qquad (16)$$

The six symmetry types of vacancy sites that are in the first coordination shell (first neighbor with the solute) or in the second coordination shell (sites accessible from the first shell by one single vacancy jump) are shown in Fig. 2. Sites that are equally distant from the solute atom S at the origin, and that have the same abscissa (x-coordinate in Fig. 2) share the same vacancy occupation probability n_i, equivalently for $n_{\bar{i}}$. Table 1 resumes the sites probability with n_{ij} where for $i \neq 0$ there is only one index i that is given in crescent order with the distance to the solute atom S in a positive abscissa, while $\bar{i}$ denote sites with negative x coordinate. For the sites in the $x = 0$ plane ($i = 0$), the sites are denoted with two indexes as n_{0j}, where the second index j is given in crescent order of the distance to the solute atom S. Table 1 denotes the number of different types of sites and the distance of them to the x axis.

The Onsager coefficients can be entirely obtained in terms of both, the free and paired specie concentrations, and the jump frequencies ω_i. For the case of binary alloys the coefficients are L_{AA}, L_{SS} and L_{AS}.

As was shown in Refs. [9,10], the Onsager coefficient for the solute specie can be written as

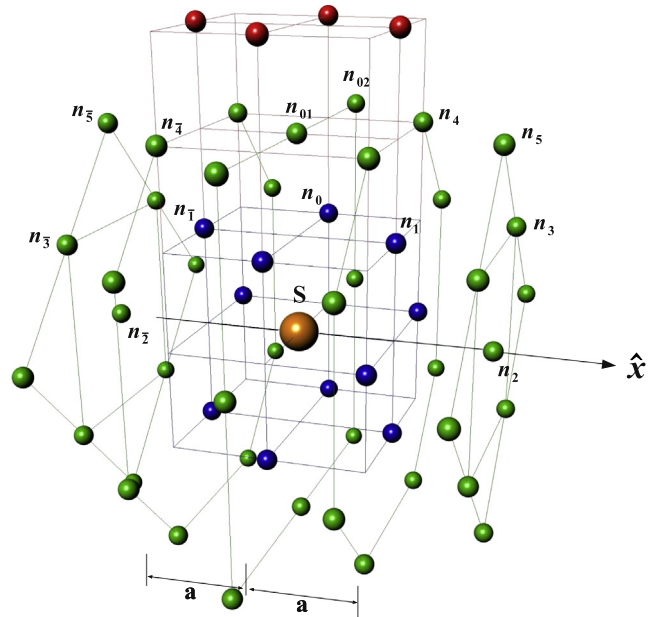Fig. 1. The five-frequency model of a solute-vacancy pair in a f.c.c. lattice.

Fig. 2. (Colors online) The coordinated shell model in f.c.c. lattice (see Ref. [23]). The different types of symmetries shown are detailed in Table 1. In the figure, blue bullets are the first twelve neighbors sites with the solute **S** at the origin. In green the 42 subsequent sites. In red, the third coordinated shell from which the vacancy never returns to the second shell.

Table 1
Probability of occurrence of the vacancy at a site of the subset n_j.

n_{ij} [23]	n_5	n_4	n_3	n_2	n_1	n_{01}	n_{02}	n_0
# of sites	4	8	4	1	4	4	4	4
separation	$2a$	$a\sqrt{2}$	0	$a\sqrt{5}$	a	$a\sqrt{2}$	$2a$	$a\sqrt{2}$

$$L_{SS} = L(\omega_2)\left\{1 - \frac{2\omega_2}{\Omega}\right\}, \tag{17}$$

were the function $L(\omega_i)$ is,

$$L(\omega_i) = N\beta c_p \omega_i \frac{s^2}{6}. \tag{18}$$

In (18) $s = a/\sqrt{2}$ is the jump length, with a is the lattice parameter for f.c.c. solvent A and c_p denotes the site fraction of solute atoms with a vacancy among their z nearest-neighbor sites. Ω in (17) is given by

$$\Omega = 2(\omega_1 + \omega_2) + 7\omega_3^\star F. \tag{19}$$

Introducing Ω (19) in L_{SS} (17), we obtain the tracer correlation factor for the solute f_S as,

$$f_S = \frac{2\omega_1 + 7\omega_3^\star F}{2(\omega_1 + \omega_2) + 7\omega_3^\star F}. \tag{20}$$

The quantity F in (20) is a function of the ratio $y = \omega_4^\star/\omega_0$ which is expressed as,

$$7(1 - F) = \frac{y(B_1 y^3 + B_2 y^2 + B_3 y + B_4)}{B_5 y^4 + B_6 y^3 + B_7 y^2 + B_8 y + B_9}. \tag{21}$$

Table 2 shows the B_i coefficients in (21) calculated by Manning [24] and Koiwa [25] using respectively exact and perturbative methods. Also following [9,10], the mixed coefficient L_{AS} is,

$$L_{AS} = L_{SA}$$
$$= 2L(\omega_2) \times \left\{3\omega_3^\star - 2\omega_1 + 7\omega_3^\star(1-F)\left(\frac{\omega_0 - \omega_4^\star}{\omega_4^\star}\right)\right\}\frac{1}{\Omega}. \tag{22}$$

While for the solvent,

$$L_{AA} = L_{AA}^{(0)} + L_{AA}^{(1)}, \tag{23}$$

with

$$L_{AA}^{(0)} = L(4\omega_1 + 14\omega_3^\star) + 2N\beta s^2 \omega_0(c_V - c_p)[1 - 7(c_S - c_p)], \tag{24}$$

and

$$L_{AA}^{(1)} = -2L(3\omega_3^\star$$
$$- 2\omega_1)\left[(3\omega_3^\star - 2\omega_1) + 7\omega_3^\star(1 - F)\left(\frac{\omega_0 - \omega_4^\star}{\omega_4^\star}\right)\right]\frac{1}{\Omega}$$
$$- 2L(3\omega_3^\star - 2\omega_1) \times \left[7\omega_3^\star(1 - F)\left(\frac{\omega_0 - \omega_4^\star}{\omega_4^\star}\right)\right]\frac{1}{\Omega}$$
$$- 2L(3\omega_3^\star)\left(\frac{\omega_0 - \omega_4^\star}{\omega_4^\star}\right)^2$$
$$\times \left[7(1 - F)(2\omega_2 + 2\omega_1 + 7\omega_3^\star)\frac{1}{\Omega}\right]. \tag{25}$$

For evaluating the L-coefficients (17), (22) and (23), two parameters are needed, namely, the fraction of unbounded vacancies $c_V' = c_V - c_p$ and the unbound solute atoms $c_S' = c_S - c_p$. They are related with the frequency jumps through the mass action equation [12],

$$\frac{c_p}{c_V' c_S'} = z\exp(-E_b/k_B T) = \frac{\omega_4^\star}{\omega_3^\star}, \tag{26}$$

where E_b is the binding energy of the solute atom with a vacancy at its nearest neighbor sites. Then, if the pairs and free vacancies are in local equilibrium and the fraction of solute c_S is much greater than both c_V and c_p, we can define the equilibrium constant K as,

$$\frac{c_p}{c_V - c_p} = zc_S \exp(-E_b/k_B T) \equiv Kc_S, \tag{27}$$

and equivalently

$$c_p = c_V\left(\frac{Kc_S}{1 + Kc_S}\right). \tag{28}$$

In the next section we present the analytical expressions for the tracer diffusion coefficients $D_A^\star$ and $D_S^\star$ in terms of the jump frequencies ω_i defined in the five-frequency model through the full set of L-coefficients expressions in (17)–(25).

4. The tracer diffusion coefficients D_A and D_S

The diffusion model here described, is validated by the comparison of present simulations with available experimental data for the tracer diffusion coefficients $D_A^\star$ and $D_S^\star$.

In the diluted limit ($c_S \to 0$) the intrinsic diffusion coefficient D_S in (8) is identical to the tracer diffusion coefficient $D_S^\star$,

$$D_S = D_S^\star(0) = \frac{k_B T}{Nc_S}L_{SS}. \tag{29}$$

Introducing L_{SS} from (17) in (29), and assuming that $c_V \gg c_p \to c_V' = c_V$ in the detailed balance Eq. (26), we obtain an expression for the tracer solute diffusion coefficient as,

$$D_S^\star(0) = \frac{s^2}{6}\omega_2\left(\frac{c_p}{c_S}\right) \times \left\{\frac{2\omega_1 + 7\omega_3^\star F}{2\omega_1 + 2\omega_2 + 7\omega_3^\star F}\right\}$$
$$= z\frac{s^2}{6}\omega_2 c_V \exp(-E_b/k_B T) \times f_S. \tag{30}$$

where $s = a/\sqrt{2}$ and $z = 12$, is the coordination number for f.c.c. lattices. In (30) the term in brackets is the solute correlation factor f_S.

On the other hand, based on Le Claire's model [12], the tracer self-coefficient $D_A^\star(c_S)$ with a diluted concentration c_S of solute atoms S, can be expressed in terms of the self diffusion coefficient $D_A^\star(0)$, of the pure A matrix and the so called solvent enhancement factor $b_{A^\star}$ as,

$$D_A^\star(c_S) = D_A^\star(0)(1 + b_{A^\star}c_S). \tag{31}$$

As was shown in Ref. [26], the self-diffusion coefficient $D_A^\star(0)$ in (31), can be obtained from expression (30) for the tracer diffusion coefficient S, by replacing all the jump frequencies ω_i by ω_0 and taking $E_b = 0$. Hence, the self-diffusion coefficient can be written as:

Table 2
Coefficients in the expression for F for the five frequency model calculated by Manning [24] and Koiwa [25].

	B_1	B_2	B_3	B_4	B_5	B_6	B_7	B_8	B_9
Ref. [24]	20	380	2062	3189	4	90	656	1861	1711
Ref. [25]	10	180	924	1338	2	40	253	596	435

$$D_A^\star(0) = z\frac{s^2}{6}\omega_0 c_V f_0, \qquad (32)$$

where f_0, the correlation factor for pure f.c.c. metals, is obtained from f_s in (20) by replacing all the jump frequencies ω_i by ω_0. Note that in (21) if $\omega_4^\star/\omega_0 = 1$, and the B_i coefficients are those in Table 2 then $7F = 5.69$ or $7F = 5.15$, respectively for the Manning [24] or Koiwa [25] descriptions. Inserting the value $7F = 5.69$ or $7F = 5.15$ in (20) we obtain $f_0 = 0.7936$ or $f_0 = 0.7814$, respectively.

At thermodynamic equilibrium the vacancy concentration $c_V = c_V^{(0)}$ is given by,

$$c_V^0 = \exp\left(-E_f^V/k_B T\right), \qquad (33)$$

where E_f^V is the formation energy of the vacancy in pure A. The entropy terms are here set to zero, which is a simplifying approximation. So that, inserting (33) in (32) we get

$$D_A^\star(0) = z\frac{s^2}{6}\omega_0 f_0 \exp\left(-\beta E_f^V\right). \qquad (34)$$

As was demonstrated by Le Claire in Ref. [12], the solvent enhancement factor, $b_{A^\star}$ in (31), depends on the properties of the solute-vacancy model. As an approximation for the five-frequency model, only valid in the context of the random alloy model [19], $b_{A^\star}$ can be calculated directly from the Onsager phenomenological coefficients L_{AS} and L_{AA} in (22) and (23) respectively, through,

$$D_A^\star = \frac{k_B T f_0}{N c_A}(L_{AA} + L_{AB}). \qquad (35)$$

Then, $b_{A^\star}$ is obtained by equating the expressions (31) and (35) for $D_A^\star$ hence,

$$\frac{k_B T}{N c_A}(L_{AA} + L_{AS}) = z\frac{s^2}{6}\omega_0 c_V(1 + b_A^\star \cdot c_S). \qquad (36)$$

Also, Belova and Murch [28] have address the problem of the enhancement of the solvent in diluted alloys giving an expression for $b_{A^\star}$ in terms of f_0 and the ratio ω_2/ω_0, up to third order in the solute concentration. The authors [28] have then obtained an excellent agreement with the theory of Moleko et al. [29].

In more concentrated alloys the understanding of the diffusion behavior requires a significantly different approach as the one developed by Van der Ven et al. in Refs. [30,31]. Recently, Van der Ven et al. [32], gave another point of view of the same transport phenomena, describing a formalism to predict diffusion coefficients of substitutional alloys from first principles restricted to vacancy mediated diffusion mechanism. This approach relies on the evaluation of Kubo–Green expressions of kinetic transport coefficients using Monte Carlo simulations.

5. Results

We present our numerical results, using a classical molecular static technique (CMST) coupled to the Monomer method [16], applied to Ni–Al and Al–U diluted alloys. In the case of the Ni–Al system, for the pure elements Ni and Al, as well as, for the cross Ni–Al term, the atomic interaction are represented by EAM potentials, developed by Mishin et al. [33], where the cross term, was fitted taking into account the available first principles data. For the Al–U system concerning to the pure elements, we use the potential developed by Zope and Mishin [34] for Al, while for U and the cross term we use the potentials reported in Ref. [35]. In this case, lattice parameters, formation energies and bulk modulus for each intermetallic compound are well reproduced. The cross potential in Ref. [35], has been fitted taking into account the available first principles data [36]. We obtain the equilibrium positions of the atoms by relaxing the structure via the conjugate

gradients technique. The lattice parameters that minimize the crystal structure energy are $a_{Ni} = 3.52$ Å for Ni and $a_{Al} = 4.05$ Å for Al. For all calculations we use a christallyte of $8 \times 8 \times 8$ of 2048 atoms, with periodic boundary conditions.

Impurity and defect relaxation, includes one substitutional Al atom in Ni or one substitutional U atom in Al, as well as, a single vacancy. Current calculations have been performed at $T = 0$ K. In this case, the entropic barrier is ignored. Our calculations are carried out at constant volume, and therefore the enthalpic barrier $\Delta H = \Delta U + p\Delta V$ is equal to the internal energy barrier ΔU.

In Table 3, we present our results for the vacancy formation energy (E_f^V) in pure Ni and Al calculated as $E_f^V = E(N - 1) + E_c - E(N)$, where $E(N)$ is the energy of the perfect lattice of N atoms, $E(N - 1)$ is the energy of the defective system, and E_c the cohesion energy. The vacancy migration barrier in perfect lattice, E_m^V, is calculated with the Monomer method [16], and the activation energy, E_Q, is then obtained as, $E_Q = E_f^V + E_m^V$.

For the case of a diluted alloy, we consider the presence of solute vacancy complexes, $C_n = S + V_n$, in which $n = 1st,2nd,3rd,\ldots$ (see the insets in Table 4) indicates that the vacancy is a n−nearest neighbors of the solute atom S. The binding energy between the solute and the vacancy for the complex $C_n = S + V_n$ in a matrix of N atomic sites is obtained as,

$$E_b = \{E(N - 2, C_n) + E(N)\} - \{E(N - 1, V) + E(N - 1, S)\}, \qquad (37)$$

where $E(N - 1, V)$ and $E(N - 1, S)$ are the energies of a crystallite containing $(N - 1)$ atoms of solvent A plus one vacancy V, and one solute atom S respectively, while $E(N - 2, C_n)$ is the energy of the crystallite containing $(N - 2)$ atoms of A plus one solute vacancy complex $C_n = S + V_n$. With the sign convention used here $E_b < 0$ means attractive solute-vacancy interaction, and $E_b > 0$ indicates repulsion.

For the alloys, we calculate the migration energies E_m using also the Monomer Method [16], a static technique to search the potential energy surface for saddle configurations, thus providing detailed information on transition events. The Monomer computes the least local curvature of the potential energy surface using only forces. The force component along the corresponding eigenvector is then reversed (pointing "up hill"), thus defining a pseudo force that drives the system towards saddles. Both, local curvature and configuration displacement stages are performed within independent conjugate gradients loops. The method is akin to the Dimer one from the literature [42], but roughly employs half the number of force evaluations which is a great advantage in ab initio calculations.

Tables 4 and 5 display, respectively for Ni–Al and Al–U, the different type of solute vacancy complexes $C_n = S + V_n$ with its binding energies E_b and with the corresponding jump frequencies. Also, the same tables, depict the possible configurations and jumps involved.

For Ni–Al, a weak binding energy, E_b, can be observed for almost all the solute-vacancy complexes, C_n, being attractive for C_1 and C_4 and repulsive for the rest of the pairs. The same behavior is observed in Al–U, although for this case, the binding energy, E_b, for the C_1 complex is strongly attractive.

Concerning with the migration barriers, summarized in Table 4, our results show that for Ni–Al, the migration barriers E_m^- are close to the perfect lattice value ($0.98eV$).

For Al–U, as can be seen in Table 5, the migration barriers are quite different from $0.65eV$, the value in perfect lattice, except for the transition $C_4 \rightarrow C_6$. In comparison with the Ni–Al case, the jump $C_1 \overset{\omega_3''}{\underset{\omega_4''}{\rightleftarrows}} C_4$, involves more than one atom, as indicated in the figure inserted in Table 5, and shown in more detail in Fig. 3. In Fig. 3, we show both, direct and indirect jumps involving

Table 3

Energies and lattice parameters for the pure f.c.c. Al and Ni and αU lattices. The first column specifies the metal, vacancy formation energy E_f^V (eV) are shown in the second column. The third column displays the migration energies E_m^V, calculated from the Monomer method [16]. In the forth column we show the lattice parameter a_A (Å). The last column displays the activation energy E_Q (eV).

Reference	Latt.	E_c (eV)	E_f^V (eV)	E_m^V (eV)	a_A (Å)	E_Q (eV)
Ni–Al						
Present work	Ni	−4.45	1.56	0.98	3.52	2.54
Voter and Chen [37]	Ni	−4.45	1.56	0.98	3.52	2.54
Ref. [33] using CMST	Ni	−4.45	1.60	1.29	3.52	2.89
Ref. [18] using VASP	Ni	−4.45	1.40	1.28	3.52	2.65
Experimental/ab initio	Ni	−4.45 [38]	1.60 [39]	1.30 [40]	3.52 [40]	2.90
Present work	Al	−3.36	0.68	0.65	4.05	1.33
Voter and Chen [37]	Al	−3.36	0.63	0.30	4.05	0.93
Ref. [33] using CMST	Al	−3.36	0.68	0.64	4.05	1.32
Experimental/ab initio	Al	−3.36 [38]	0.68 [39]	0.65 [40]	4.05 [41]	1.33
Al–U						
Present work	Al	−3.36	0.65	0.65	4.05	1.30
Ref. [34] using CMST	Al	−3.36	0.68	0.63	4.05	1.31
Present work	αU	−5.77	1.36	0.23	$a_U = 2.77$ $b_U = 6.07$ $c_U = 4.94$	1.59

Table 4

Jumps and frequencies in Ni–Al. The first column denotes $C_n = S + V_n$ where V_n means that the vacancy is n nearest neighbor of the solute. Binding energy E_b is shown in the second column. The jumps are depicted in the third column, while the forth column describes the jump frequency ω_i and the configurations involved in each jump. Migration energies E_m for direct and reversed jumps are written in the fifth and sixth column respectively.
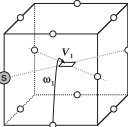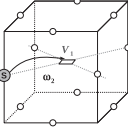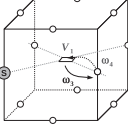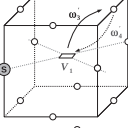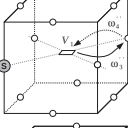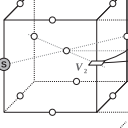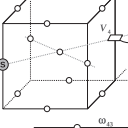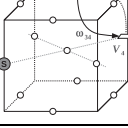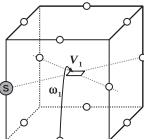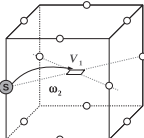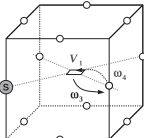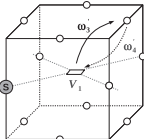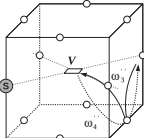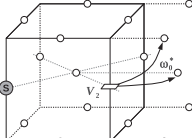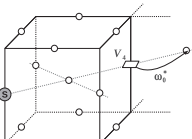
$C_n = S + V_n$	E_b (eV)	Config. (F_n)	ω_i	$E_m^{\rightarrow}$ (eV)	$E_m^{\leftarrow}$ (eV)
C_1	−0.06		$C_1 \underset{\omega_1}{\overset{\omega_1}{\rightleftarrows}} C_1$	1.09	1.09
C_{1S}	−0.06		$C_{1S} \underset{\omega_2}{\overset{\omega_2}{\rightleftarrows}} C_{1S}$	0.97	0.97
C_2	0.03		$C_1 \underset{\omega_4}{\overset{\omega_3}{\rightleftarrows}} C_2$	0.98	0.89
C_3	0.03		$C_1 \underset{\omega'_4}{\overset{\omega'_3}{\rightleftarrows}} C_3$	0.99	0.91
C_4	−0.001		$C_1 \underset{\omega''_4}{\overset{\omega''_3}{\rightleftarrows}} C_4$	0.96	0.90
C_5	0.034		$C_2 \underset{\omega_0^{\star}}{\overset{\omega_0^{\star}}{\rightleftarrows}} C_5$	0.89	0.98
C_6	0.031		$C_4 \underset{\omega_0^{\star}}{\overset{\omega_0^{\star}}{\rightleftarrows}} C_6$	0.98	0.98
C_7	−0.001		$C_2 \underset{\omega_{34}}{\overset{\omega_{43}}{\rightleftarrows}} C_5$	1.01	0.98

Table 5
Jumps and frequencies in $Al-U$. The columns description is the same as in Table 4.

$C_n = S + V_n$	E_b (eV)	Config. (F_n)	ω_i	$E_m^{\rightarrow}$ (eV)	$E_m^{\leftarrow}$ (eV)
C_1	−0.139		$C_1 \underset{\omega_1}{\overset{\omega_1}{\rightleftarrows}} C_1$	0.81	0.81
C_{1S}	−0.139		$C_{1S} \underset{\omega_2}{\overset{\omega_2}{\rightleftarrows}} C_{1S}$	0.48	0.48
C_2	0.004		$C_1 \underset{\omega_4}{\overset{\omega_3}{\rightleftarrows}} C_2$	0.61	0.47
C_3	0.037		$C_1 \underset{\omega_4'}{\overset{\omega_3'}{\rightleftarrows}} C_3$	0.65	0.48
C_4	0.019		$C_1 \underset{\omega_4''}{\overset{\omega_3''}{\rightleftarrows}} C_4$	0.73	0.58
C_5	0.015		$C_2 \underset{\omega_0^{\star}}{\overset{\omega_0^{\star}}{\rightleftarrows}} C_5$	0.59	0.58
C_6	−0.003		$C_4 \underset{\omega_0^{\star}}{\overset{\omega_0^{\star}}{\rightleftarrows}} C_6$	0.63	0.65

respectively one or two atoms. For the jump (1), the atom labeled 3 is dragged by the atom labeled 1 to the vacancy site. The jump (2) is the reverse of jump (1). While for the direct jump (3), the atom 1 jumps towards the vacancy, although, it is a high energy jump (see Fig. 4).

As the direct jump (3) has lower probability of occurrence than the indirect jump (1), then present calculations of frequencies are performed using the values corresponding to this last one, that is 0.73 eV and 0.58 eV, to compute ω_3'' and ω_4'', respectively, and using $v^{\star}$ from Table 7.

Although the jump $C_1 \rightarrow C_4$ in $Al-U$ involves two atoms it is not a successive jump. It is indeed a single jump which involves two atoms, that is, there is a single saddle point for the whole jump. The monomer method here employed is able to find both saddle point energy and configuration.

In Table 6, we show the migration barriers for more distant neighbors pairs than the forth. As can be seen, the values obtained are close to 0.65 eV, the migration barrier in the perfect crystal.

In order to compute ω_i, we use the conventional treatment formulated by Vineyard [11], that corresponds to the classical limit, where the vibrational prefactors, $v^{\star}$, do not depend on the temperature, that is
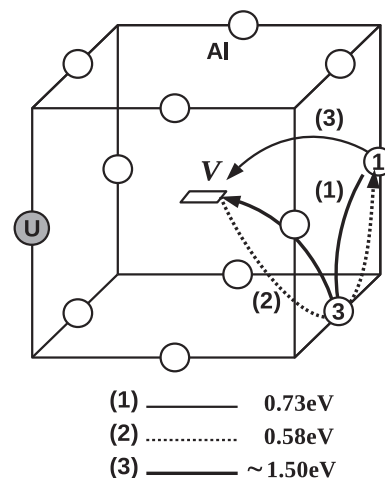

Fig. 3. Single jump involving two atoms in $Al-U$. In jump (1) the atom labeled 1 takes the place of atom 3, which is dragged by the atom 1 towards the vacancy V. Jump (2) is the reverse of jump (1). We also depict a direct jump (3) which is a high energy jump involving only the atom 1.
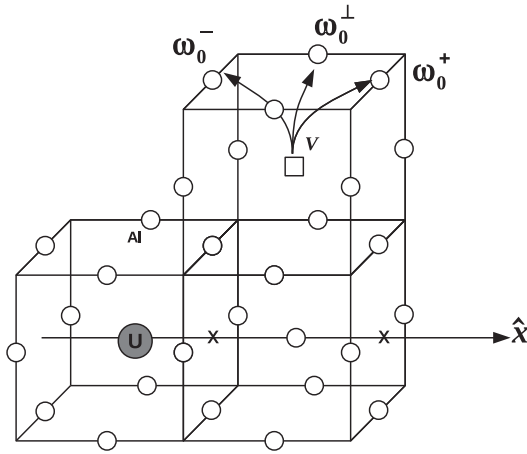
Fig. 4. Vacancy jumps beyond the second coordinated shell. The superscripts $(\perp, \mp)$ on ω_0 implies vacancy jumps perpendicular to, backward or forward $\mp\hat{x}$ respectively.

$$\omega_i = v^\star \exp(-E_m^i/k_B T), \tag{38}$$

with

$$v^\star = \frac{\prod_{i=1}^{3N} v_i^l}{\prod_{i=1}^{3N-1} v_i^S}, \tag{39}$$

and E_m^i is the migration barrier. In (39), v_i^l and v_i^S are the frequencies of the normal vibrational modes at the initial and saddle points, respectively. That is, v_i^l refers to the vibrational frequencies of the nearest neighbors $X–V$ pair (X = Ni, Al, U) and v_i^S refers to the saddle configuration for the S-vacancy exchange, the product does not include the unstable mode. Note that, Eq. (39) is based on calculation of the frequencies of the normal vibrational modes. This normal modes can involve only one atom or being collective modes. Hence it is also applicable to the single jump $C_1 \rightarrow C_4$ in $Al–U$ involving two atoms.

In Table 7 we report the calculated attempt frequencies.

Once the jump frequencies in the five-frequency model have been computed, the diffusion coefficients are calculated using analytical expressions in terms of the temperature. It is important to note the discrepancy between the classical and the quantum description concerning to the evaluation of ω_i [43]. Although these discrepancies are large in the low-temperature range the quantum value gradually converges to the classical one at temperatures higher than room temperature [43]. Hence, here we employ a classical description.

Table 8 presents the calculated frequencies (38) for two different temperatures with the migration energies taken from Tables 4 and 5. Using a different approach based on the Wert and Zener model [45], Zacherl et al. [18,46], have studied diffusion in Ni based diluted alloys using a temperature dependent frequency prefactor.

Table 6
Jumps beyond the second coordinated shell. The binding energies are shown in the second column. The third column denoted the frequency rate, where the superscripts $(\perp, \mp)$ on ω_0 implies vacancy jumps perpendicular $\perp$, backward $-$ or forward $+$ in respect to the $\hat{x}$ direction. Migration energies are shown in column four and five.

$C_n = S + V_n$	E_b (eV)	ω_i	$E_m^{\rightarrow}$ (eV)	$E_m^{\leftarrow}$ (eV)
C_7	0.002	$C_7 \overset{\omega_0^\perp}{\rightarrow} C_{10}$	0.61	0.64
C_8	0.015	$C_8 \overset{\omega_0^-}{\rightarrow} C_{11}$	0.64	0.61
C_9	0.002	$C_{12} \overset{\omega_0^+}{\rightarrow} C_{12}$	0.61	0.64

From the calculated jump frequencies, then the tracer correlation factors f_S and the solvent enhancement factors $b_{A\star}$ can be obtained from (20) and (36), respectively. They are shown in Table 9, together with the jump frequencies ratios calculated according to the five-frequency model.

The solute correlation factor, f_S, obtained from (20), is also shown in Figs. 5 and 6 in terms of the inverse of the absolute temperature, respectively for $Ni–Al$ and $Al–U$, together with the F factor from (21).

In Table 9, the solvent-enhancement factors, $b_{A\star}$, is obtained from (36) and depicted in Figs. 7 and 8, respectively for $Ni–Al$ and $Al–U$, as a function of the temperature. It must be taken into account that the effect of $b_{A\star}$ on the tracer self-diffusion coefficient $D_A^\star(c_S)$, must be multiplied by the solute concentration c_S, which is low for diluted alloys, hence $D_A^\star(c_S)$ is similar to $D_A^\star(0)$.

The Onsager and diffusion coefficients were calculated for a solute molar fraction $c_S = 4.9 \times 10^{-4}$, for both alloys, which corresponds to $n_{Al} = 4.53 \times 10^{19}$ cm^{-3} at./cm^3 for $Ni–Al$ and $n_U = 3.01 \times 10^{19}$ cm^{-3} at./cm^3 for $Al–U$.

From L_{AS} and L_{SS}, we also calculate the vacancy wind coefficient G as in Ref. [15]. The L_{VS} coefficient, which provides essential information about the flux of S atoms induced by the vacancy flow can be defined in terms of the Onsager coefficients L_{SS} and L_{AS}, respectively in (17) and (22) as,

$$L_{VS} = -(L_{SS} + L_{SA}) = -L_{SS}(G + 1), \tag{40}$$

where G is defined as the vacancy wind coefficient. The final expression is given by,

$$\begin{aligned} G &= \frac{L_{AS}}{L_{SS}} \\ &= \frac{1}{(2\omega_1 + 7\omega_3^\star F)}\left[6\omega_3^\star - 4\omega_1 + 14\omega_3^\star(1 - F)\left(\frac{\omega_0 - \omega_4^\star}{\omega_4^\star}\right)\right]. \end{aligned} \tag{41}$$

The G parameter in (41) accounts for the coupling between the flux of species J_A and J_S, through the vacancy flux, J_V [47]. The results are presented in Figs. 9 and 10, for $Ni–Al$ and $Al–U$ systems respectively. In Fig. 9, the vacancy wind parameter verifies $G > -1$ for $Ni–Al$ in the full range of temperatures considered, while for $Al–U$, Fig. 10 shows that $G > -1$ only above 550K.

In the case where $G < -1$, L_{VS} is positive, then the vacancy and the solute diffuse in the same direction as a complex specie [15]. This transport phenomena could occur in $Al–U$ at lower temperatures, due to the strong binding of the C_1 pair, while is unlikely to occur for Al in Ni by the opposite argument.

The full set of L-coefficients, are displayed in Figs. 11 and 12, against the inverse of the temperature for the $Ni – Al$ and $Al–U$, respectively. We see that for the $Ni–Al$ case the L-coefficients follow an Arrhenius behavior, which implies a linear relation between the logarithm of L-coefficients against the inverse of the temperature (see Fig. 11). For $Al – U$ we can appreciate a deviation of the L_{AlU} coefficient from the Arrhenius law at high temperatures (see Fig. 12).

In Fig. 12, the cross $L_{AlU} = L_{UAl}$ coefficient is negative in all the temperature range considered.

Now, we are in position to obtain the tracer diffusion coefficients $D_A^\star$ and $D_B^\star$. First, we present the ratio of the calculated tracer diffusion coefficients $D_S^\star/D_A^\star$ as a function of the inverse of the temperature for the $Ni – Al$ and $Al – U$ in Figs. 13 and 14, respectively.

In Figs. 13 and 14, we also show the ratio between the intrinsic diffusion coefficients, D_S/D_A (in stars symbols) calculated from (7) and (8).

The tracer diffusion coefficients $D_S^\star$ and $D_A^\star$, calculated from (30) and (31), are shown in Figs. 15 and 16 respectively for $Ni – Al$ and $Al – U$. It is important to perform a comparison between

Table 7
Attempt frequencies $v^\star$ in (38) in *THz* unit. We compare present calculations with results using the density functional theory (DFT) respectively in the local density (LDA) and generalized gradient (GGA) approximations, and from Monte Carlo (MC) simulations.

Ref.	$Ni \rightarrow V$ in *Ni*	$Al \rightarrow V$ in *Ni*	Ref.	$Al \rightarrow V$ in *Al*	$U \rightarrow V$ in *Al*
Present work	23.7	30.8	Present work	19.56	8.25
[26] DFT	4.48	–	[14] DFT (LDA)	20.79	–
[27] B2-*NiAl* MC	50.7	47.7	[14] DFT (GGA)	22.51	–
			[44] CMST	22.60	–

Table 8
Vacancy jump frequencies ω_i calculated from (38) using the description of vineyard. The symbol ($\star$) indicates effective frequencies.

	Ni–Al		*Al–U*	
	$T_1 = 800$ K	$T_2 = 1700$ K	$T_1 = 300$ K	$T_2 = 600$ K
ω_0	1.6×10^7	2.9×10^{10}	2.9×10^2	7.6×10^7
ω_1	3.2×10^6	1.4×10^{10}	4.8×10^{-1}	3.1×10^6
ω_2	2.4×10^7	4.1×10^{11}	7.1×10^4	7.7×10^8
$\omega_3^\star$	1.6×10^7	2.9×10^{11}	4.5×10^2	8.3×10^7
$\omega_4^\star$	4.9×10^8	5.0×10^{11}	1.7×10^5	1.7×10^9

Table 9
Solvent enhancement and solute correlated factors for *Ni–Al* and *Al–U* at different temperatures. The first two columns describe the alloy and the temperature range considered. For the solvent enhancement factor $b_{A^\star}$ (column three), and for the solute correlated factor f_S (column four). The last tree columns describe the jump frequency ratios of the solute-vacancy interaction.

Alloy	T/K	$b_{Ni^\star}$	$f_{Al^\star}$	ω_2/ω_1	$\omega_3^\star/\omega_1$	$\omega_4^\star/\omega_0$
Ni–Al	700	−23.4	0.61	7.9	5.6	3.6
	800	−19.0	0.62	7.4	4.9	3.1
	900	−14.2	0.63	6.1	4.1	2.7
	1000	−10.9	0.64	5.2	3.6	2.5
	1100	−8.7	0.65	4.6	3.2	2.3
	1200	−7.2	0.66	4.1	2.9	2.1
	1300	−5.9	0.67	3.8	2.7	2.0
	1400	−5.1	0.67	3.5	2.5	1.9
	1500	−4.4	0.68	3.3	2.3	1.8
	1600	−3.8	0.68	3.1	2.2	1.8
	1700	−3.3	0.69	2.9	2.1	1.7
Alloy	T/K	$b_{Al^\star}$	$f_U^\star$	ω_2/ω_1	$\omega_3^\star/\omega_1$	$\omega_4^\star/\omega_0$
Al–U	300	-6.7×10^3	6.4×10^{-3}	147589.5	936.2	151.5
	350	-2.9×10^3	1.4×10^{-2}	23826.5	333.8	72.2
	400	-1.6×10^3	2.7×10^{-2}	6068.2	155.3	41.4
	450	-1.0×10^3	4.5×10^{-2}	2094.4	86.2	26.9
	500	-6.7×10^2	6.8×10^{-2}	894.3	53.9	19.0
	550	-4.8×10^2	9.6×10^{-2}	445.7	36.9	14.4
	600	-3.6×10^2	0.13	249.5	26.9	11.3
	650	-2.8×10^2	0.16	152.7	20.7	9.3
	700	-2.2×10^2	0.20	100.2	16.5	7.8
	750	-1.8×10^2	0.24	69.6	13.6	6.8
	800	-1.4×10^2	0.28	50.6	11.5	5.9
	850	-1.2×10^2	0.32	38.2	9.9	5.3
	900	-1.0×10^2	0.35	29.7	8.9	4.8

Fig. 5. Solute correlation factor $f_{Al^\star}$, obtained from (20), in the *Ni–Al* system as a function of the temperature in filled squares. The *F* factor in (21), is denoted with filled circles.

Fig. 6. Same as Fig. 5 for *Al–U*.

$$D_A^{\star,Exp} = D_A^0 \exp(-Q_A/RT), \qquad (42)$$

theoretical results obtained in present work with reliable experimental data. We have verified that the tracer self diffusion coefficient $D_A^\star(c_S)$ for a diluted alloy is practically equal to that for the pure solvent $D_A^\star(0)$ (i.e., $D_A^\star(c_S) \simeq D_A^\star(0)$).

Hence, we can test our results for $D_A^\star(c_S)$ with available experimental data in pure solvents.

In this respect, Campbell et al. [48], from a statistical analysis performed using weighted mean statistic, have determined a consensus estimators which best represents all known self diffusion available experimental data for pure solvent, $D_A^{\star,Exp}$.

The estimator $D_A^{\star,Exp}$ corresponds to the experimental self-diffusivity of species A in pure A and is expressed in the form [48],
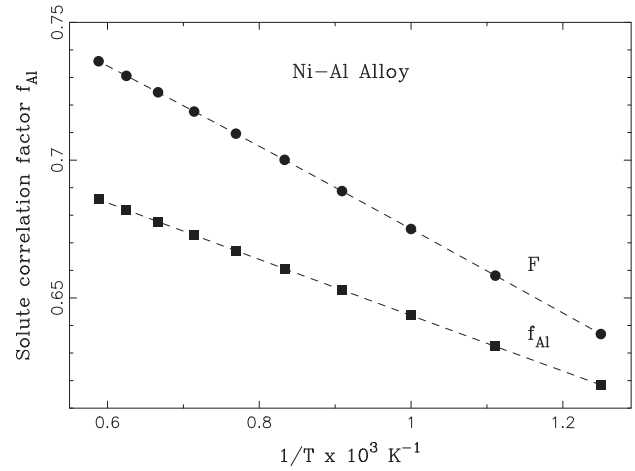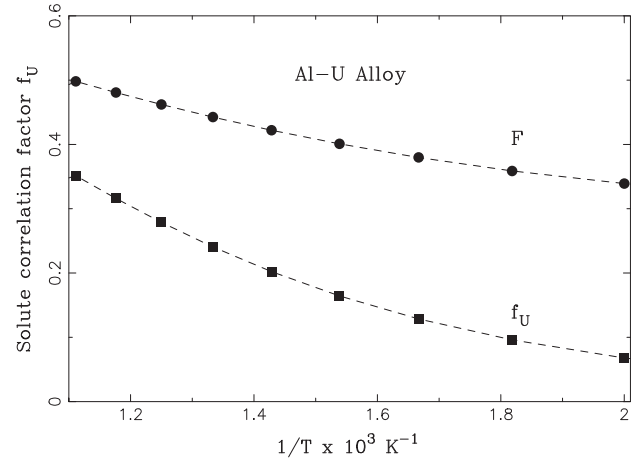
where R is the ideal gas constant, T is the absolute temperature, while the values for D_A^0 and Q_A in pure *Ni* and *Al*, are taken from Ref. [48], and are displayed in Table 10.

In order to perform a comparison of our results for $D_A^\star(c_S)$ with available experimental data in pure solvents, in Figs. 15 and 16, we display the calculated *Ni* and *Al* tracer self-diffusion coefficients (in filled circles and dashed lines), together with the consensus estimator $D_A^{\star,Exp}$ represented by solid lines. As can be observed, $D_A^{\star,Exp}$ fits well with the values of $D_A^\star$ calculated in the present work.

For the *Ni–Al* system, Fig. 15 also displays the tracer solute diffusion coefficient, our calculations (in open squares) are displayed together with experimental data for $T = [914\text{–}1212]$ °C [49] and
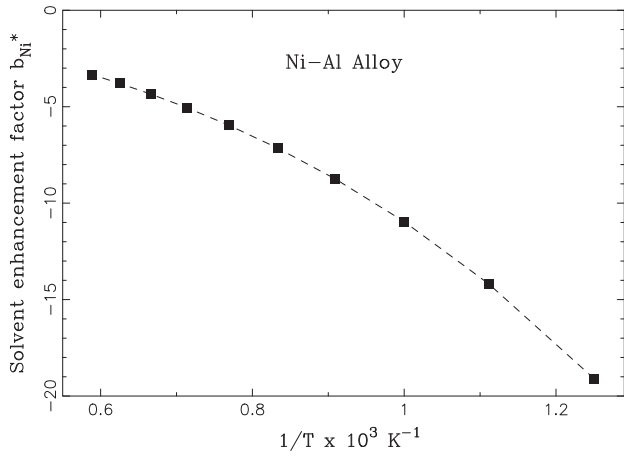
Fig. 7. Solvent-enhancement factor b_{Ni} obtained from (36), for the *Ni–Al* system as a function of the temperature.

Fig. 8. Solvent-enhancement factor b_{Al} obtained from (36), for the *Al–U* system as a function of the temperature.
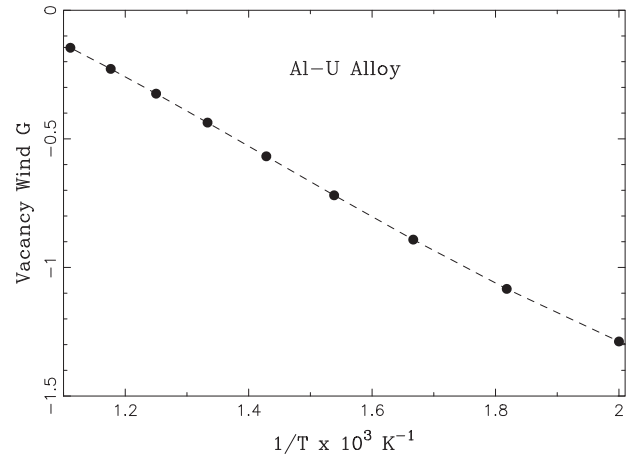

Fig. 9. The vacancy wind parameter *G* in (41): Ratio of the Onsager phenomenological coefficients of *Al* in *Ni* calculated from (17) and (22) *vs* $1/T$.
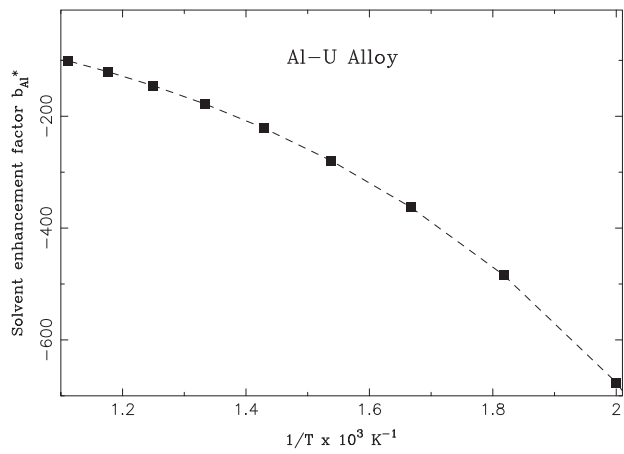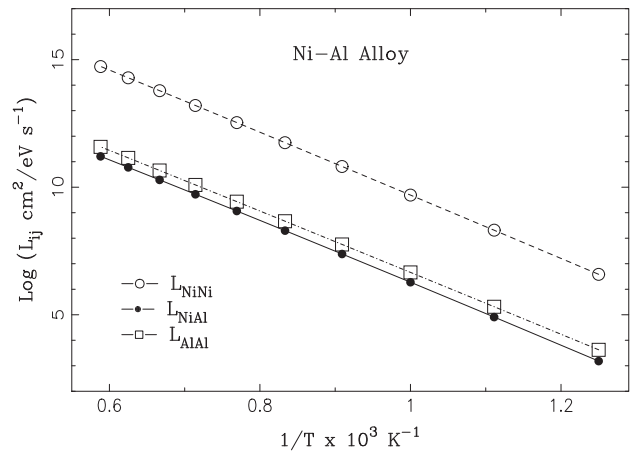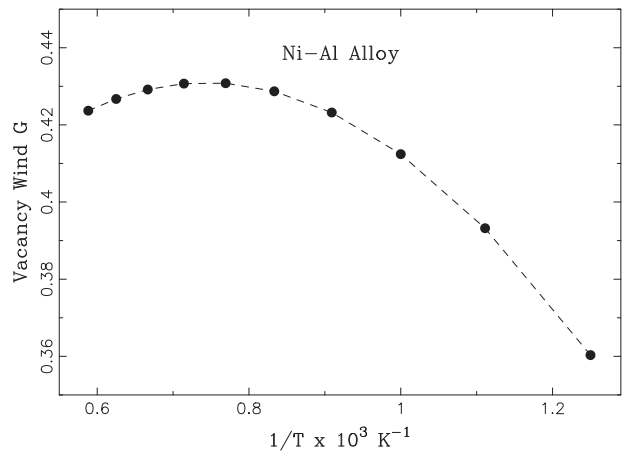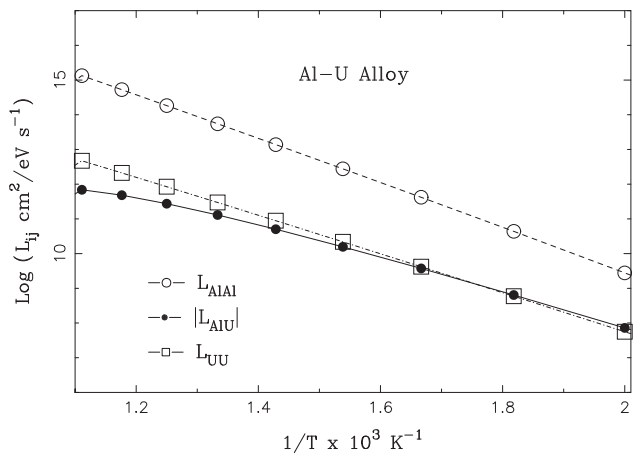

Fig. 10. The vacancy wind parameter *G* in (41): Ratio of the Onsager phenomenological coefficients of *U* in *Al* calculated from (17) and (22) *vs* $1/T$.

Fig. 11. Onsager phenomenological coefficients *vs* $1/T$ for the *Ni–Al* system. Squares denote L_{AlAl}, empty circles denote L_{NiNi} while L_{NiAl} is described with filled circles. The coefficients were calculated from (17), (22) and (23).

Fig. 12. Onsager phenomenological coefficients *vs* $1/T$ for the *Al–U* system. Squares denote L_{UU}, empty circles denote L_{AlAl} while $|L_{UAl}|$ is described with filled circles. The coefficients were calculated from (17), (22) and (23).

$T = [1372–1553]\,°C$ [50] with stars and cruxes respectively. In open triangles, we also show the experimental results obtained by Yamamoto et al. for inter-diffusion in a $\zeta - 12\%$ mass *Al–Ni* alloy in the temperature range of $T = [1273–1573]\,°C$.

With respect to the *Al–U* system, experimental values for the *U* diffusion coefficient in *Al* [4] at infinite dilution have been obtained by Housseau et al. [4]. In Ref. [4], the authors have obtained the
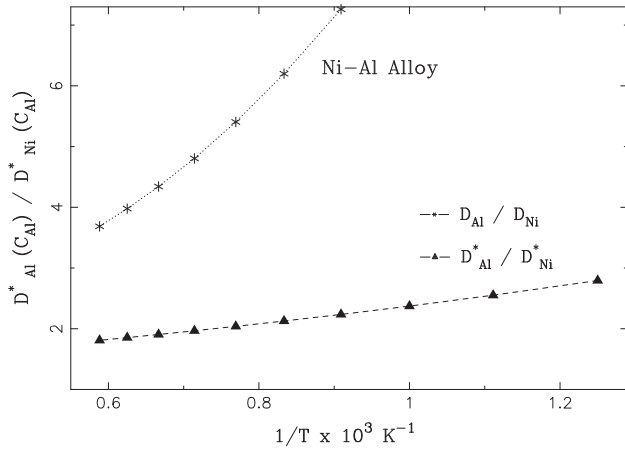
Fig. 13. Ratio of the tracer diffusion coefficient $D_{Ni}^\star/D_{Al}^\star$ in Ni–Al vs 1/T. The ratio between the intrinsic diffusion coefficients, D_S/D_A calculated from (7) and (8), is also shown with symbols in asterisk and dashed line.
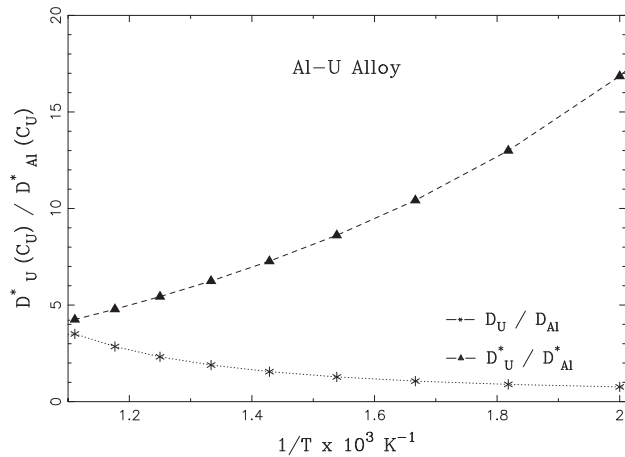

Fig. 14. Ratio of the tracer diffusion coefficient $D_U^\star/D_{Al}^\star$ in Al–U) vs 1/T. The ratio between the intrinsic diffusion coefficients, D_S/D_A calculated from (7) and (8), is also shown in stars.
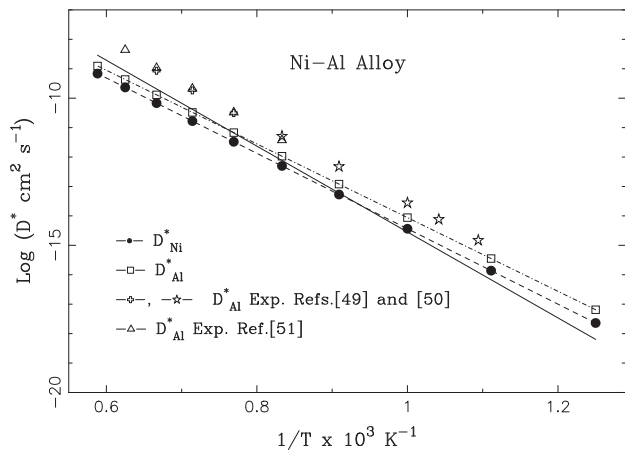

Fig. 15. Tracer diffusion coefficients of Al ($D_{Al}^\star$ in open squares) and Ni ($D_{Ni}^\star$ in filled circles) in the alloy, calculated from (30) and (31), respectively. Solid line represents the best estimative of the pure Ni self-diffusion coefficient $D_{Ni}^{\star,Exp}$, taken from Campbell work [48]. Available experimental data, for the Al diffusion coefficient in the alloy, are displayed with stars [49] and cruxes [50]. In open triangles results from Ref. [51] for the solute tracer diffusion coefficient in a $\zeta - 12\%$ mass NiAl compound in the temperature range of $T = [1273–1573]$ °C.

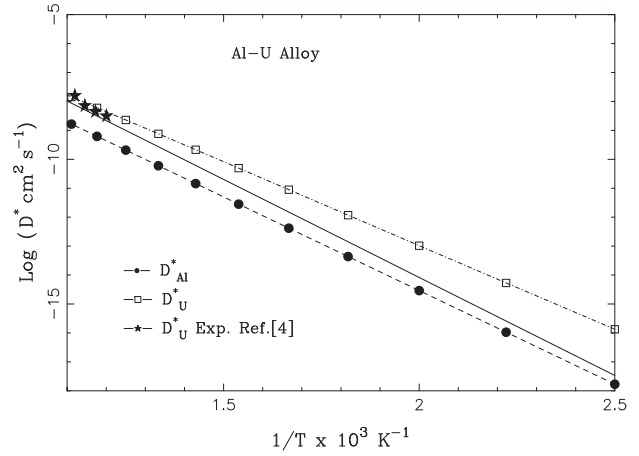**Fig. 16.** Tracer diffusion coefficients of U ($D_U^\star$ in open squares) and Al ($D_{Al}^\star$ in filled circles) in the alloy, calculated from (30) and (31), respectively. Solid line represents the best estimative of the pure Al self-diffusion coefficient $D_{Al}^{\star,Exp}$, taken from Campbell work [48]. Available experimental data, for the U diffusion coefficient in the alloy [4], are displayed with filled stars.

Table 10
Parameters involved in the expression for the self-diffusion consensus fit $D_A^{\star,Exp}$, where the parameter A indicates Ni or Al hosts. The first column denotes the reference where the values were taken from. The solvent lattice is indicated in the second column. The third and fourth columns denote the pre-exponential factor, D_A^0, and the activation energy, Q_A, for Eq. (42) respectively. The range of temperatures of the description is referred in column five. The values were taken from Campbell work [48].

Ref.	Lattice	D_A^0 (cm^2 s^{-1})	Q_A (kJ/mol)	T (°C)
[48]	Ni	1.1	279.35	[769 − 1667]
[48]	Al	0.292	129.7	[357 − 833]

diffusion parameters from the fit of their experimental permeation curves with the solution of the diffusion equation,

$$\frac{\partial C(x,t)}{\partial t} = D_U \frac{\partial^2 C(x,t)}{\partial x^2}, \tag{43}$$

with boundary condition $x = 0$; $C(0,t) = S_0$, where S_0 is the maximum solubility of the diffusing specie in the alloy. They have proposed a solution for Eq. (43) as,

$$C(x,t) = S_0[1 - erf(x/2\sqrt{D_U t}]. \tag{44}$$

Then the values of D_U and S_0 are obtained by fitting the experimental permeation curves with an expression of the form (44).

The obtained diffusion parameters, taken from Ref. [4], are shown in Table 11, for different temperatures and U concentrations, c_U. In their work [4], the authors have concluded that, at infinite dilution, the dissolution of precipitates do not disturb the U process diffusion in Al.

In Fig. 16, we establish a comparison of our calculations for $D_U^\star$ with the experimental data in Table 11, for a molar Uranium concentrations $c_U = 2 \times 10^{-4}$. We see that, experimental values (filled stars) in the temperature range of [560−620] °C are in perfect agreement with $D_U^\star$ obtained with the here described procedure. In the temperature range where there are available experimental data, the U mobility is mainly due to direct interchange between the U atom and the vacancy.

On the other hand, the diffusion of U in Al was also calculated in a study of the maximum rate of penetration of U into Al, in the temperature range [473−663] °C [5]. The maximum penetration coefficient values in Ref. [5] were, $K_T = x^2/t = 1.3 \times 10^{-4}, 8.8 \times 10^{-5}$ and 1.1×10^{-8} cm^2/s for 473 °C,523 °C and 663 °C, respectively. From

Table 11
Diffusion of U in Al, for different temperatures (1st column) and U molar concentrations c_U.

T (°C)	Uranium diffusion coefficient D_U ($\times 10^8$ cm^2 s^{-1})			
	$c_U = 2 \times 10^{-3}$	$c_U = 9 \times 10^{-4}$	$c_U = 2 \times 10^{-4}$	$c_U = 6 \times 10^{-7}$
620	1.60 ± 0.20	1.5 ± 0.15	1.56 ± 0.15	1.62 ± 0.16
600	0.78 ± 0.08	0.68 ± 0.07	0.70 ± 0.15	0.65 ± 0.07
580	0.55 ± 0.12	0.70 ± 0.12	0.44 ± 0.15	0.67 ± 0.10
560	0.40 ± 0.10	0.35 ± 0.10	0.31 ± 0.10	0.33 ± 0.10

the expression $K = K_0 \exp^{-Q/RT}$, the activation energy Q was $Q = 14.300$ in cal per mole in the temperature range of $[473-663]$ °C, where R is expressed in calories per $1/$°C per mole, and K_0 is a proportionality constant. The plot $\ln K$ vs $1/T$ provides a convenient basis for expressing and comparing penetration coefficients.

As a final comment, a recent work by Leenaers et al. [52], presents a great quantity of experimental findings for a real system, where the present model can also be applied.

Also performed but not shown here, for the $Ni-Al$, we have reproduced all the microscopical parameters with 100 atoms using the classical molecular static technique and the SIESTA code coupled to the Monomer method [17].

In the literature several researchers have studied the solvent atom-vacancy exchange in terms of the jump frequencies ω_i and f_0, in the framework of the random alloy model, as for example in Ref. [53]. The authors have performed an extensive Monte Carlo study of the tracer correlation factors in simple cubic, b.c.c. and f.c.c. binary random alloys. On the other hand, the kinetic formalism of Moleko et al. [29], also describes the behavior of the tracer correlation factors for slow and faster diffusers.

6. Concluding remarks

In summary, in this work we present the general mechanism based on non-equilibrium thermodynamics and the kinetic theory, to describe the diffusion behavior in f.c.c diluted alloys.

Non equilibrium thermodynamic, through the flux equations, relates the diffusion coefficients with the Onsager tensor, while the Kinetic Theory relates the Onsager coefficients in terms of microscopical magnitudes. In this way we are able to write expressions for the diffusion coefficients only in terms of microscopic magnitudes, i.e. the jump frequencies.

The five frequency model has also been of great utility in order to discriminate the relevant jump frequencies, evaluated from the migration barriers under the harmonic approximation in the context of the conventional treatment by Vineyard corresponding to the classical limit. Hence, we have calculated the full set of phenomenological coefficients from which the full set of diffusion coefficients are obtained through the flux equation.

In this respect, the jump frequencies have been calculated from the migration barriers which are obtained with an economic static molecular techniques (CMST) namely the monomer method, that searches saddle configurations efficiently.

Although in this work we have performed the treatment for the case of f.c.c. latices where the diffusion is mediated by vacancy mechanism, a similar procedure can be adopted for other crystalline structures or different diffusion mechanism (for example, interstitials).

We have exemplified our calculations for the particular cases of diluted $Ni-Al$ and $Al-U$ f.c.c. binary alloys. We have found that the tracer diffusion coefficient are in very good agreement with the available experimental data, for both alloys.

Present calculations show that qualitatively a vacancy drag mechanism is unlikely to occur for the $Ni-Al$ system. In the case of $Al-U$, a vacancy drag mechanism could occur at temperatures below 550 K, while above this temperature the solute migrates by a direct interchange mechanism with the vacancy, such as was corroborated in the comparison with the available experimental data.

We have demonstrated that, the CMST is appropriate in order to describe the impurity diffusion behavior mediated by a vacancy mechanism in f.c.c. alloys. This opens the door for future works in the same direction where a similar procedure will be used that includes interstitial defects.

Acknowledgments

References

[1] http://www.rertr.anl.gov/.
[2] A.M. Savchenko, A.V. Vatulin, I.V. Dobrikova, G.V. Kulakov, S.A. Ershov, Y.V. Konovalov, Proc. of the International Meeting of the RERTR, S12-5, 2005.
[3] M.I. Mirandou, S.F. Aricó, S.N. Balart, L.M. Gribaudo, Mater. Charact. 60 (2009) 888.
[4] N. Housseau, A. Van Craeynest, D. Calais, J. Nucl. Mater. 39 (2) (1971) 189–193.
[5] T.K. Bierlein, D.R. Green, The diffusion of Uranium into aluminium Physical Metallurgy Unit Metallurgy Research, 1955. www.osti.gov/scitech/servlets/purl/4368963.
[6] F. Brossa, H.W. Sheleicher, R. Theisen, Proceeding of the Symposium: New Nuclear Materials including Non-metalic Fuells, Prague – July 1–5, vol. II. Edited by I.A.E.A, 1963.
[7] M.I. Pascuet, V.P. Ramunni, J.R. Fernández, Phys. B: Condens. Matter 407 (16) (2011) 3295–3297.
[8] V.P. Ramunni, M.I. Pascuet, J.R. Fernández, Proc. of MMM 2010, Microstructure Modeling, 2010, pp. 719–722.
[9] A.R. Allnatt, J. Phys. C: Solid State Phys. 14 (1981) 5453–5466.
[10] A.R. Allnatt, J. Phys. C: Solid State Phys. 14 (1981) 5467–5477.
[11] G.H. Vineyard, J. Phys. Chem. Solids 3 (1957) 121.
[12] A.D. Le Claire, J. Nucl. Mater. 69–70 (1978) 70–96.
[13] M. Mantina, Y. Wang, L.Q. Chen, Z.K. Liu, C. Wolverton, Acta Mater. 57 (2009) 4102–4108.
[14] M. Mantina, Y. Wang, R. Arroyave, L.Q. Chen, Z.K. Liu, C. Wolverton, Phys. Rev. Lett. 100 (2008) 215901.
[15] S. Choudhury, L. Barnard, J.D. Tucker, T.R. Allen, B.D. Wirth, M. Asta, D. Morgan, J. Nucl. Mater. 411 (1-3) (2011) 1–14.
[16] V.P. Ramunni, M.A. Alurralde, R.C. Pasianot, Phys. Rev. B 74 (2006) 054113.
[17] R.C. Pasianot, R.A. Pérez, V.P. Ramunni, M. Weissmann, J. Nucl. Mater. 392 (1) (2009) 100–104.
[18] S.L. Shang, D.E. Kim, C.L. Zacherl, Y. Wang, J. Appl. Phys. 112 (2012) 053515.
[19] A.R. Allnatt, A.B. Lidiard, Atomic Transport in Solids, Cambridge University Press, 2003. Ed.
[20] R.E. Howard, A.B. Lidiard, Rep. Prog. Phys. 27 (1964) 161.
[21] G.E. Murch, Z. Qin, Defect Diffusion Forum 109 (1994) 1–18.
[22] Th. Heumann, J. Phys. F: Metal Phys. 9 (10) (1979) 1997–2010.
[23] J.L. Bocquet, Acta Metall. 22 (1974).
[24] J.R. Manning, Phys. Rev. 136 (1964) A175846.
[25] M. Koiwa, S. Ishioka, Philos. Mag. A47 (1983) 927.
[26] J.D. Tucker, R. Najafabadi, T.R. Allen, D. Morgan, J. Nucl. Mater. 405 (2010) 216–234.
[27] S. Divinski, Chr. Herzig, Intermetallics 8 (2000) 1357–1368.
[28] I.V. Belova, G.E. Murch, Philos. Mag. A 83 (3) (2003) 393–399.

[29] L.K. Moleko, A.R. Allnatt, E.L. Allnatt, Philos. Mag. A 59 (1989) 141.
[30] A. Van der Ven, G. Ceder, Phys. Rev. Lett. 94 (2005) 045901.
[31] A. Van der Ven, J.C. Thomas, Q.C. Xu, B. Swoboda, D. Morgan, Phys. Rev. B 78 (2008) 104306.
[32] A. Van der Ven, Hui-Chia Yu, G. Ceder, Katsuyo Thornton, Progr. Mater. Sci. 55 (2010) 61–105.
[33] Y. Mishin, D. Farkas, M.J. Mehl, D.A. Papaconstantopoulos, Phys. Rev. B 59 (1999) 3393.
[34] R. Zope, Y. Mishin, Phys. Rev. B 68 (2003) 24102.
[35] M.I. Pascuet, G. Bonni, J.R. Fernández, J. Nucl. Mater. 424 (2012) 158–163.
[36] P.R. Alonso, J.R. Fernández, P.H. Gargano, G.H. Rubiolo, Phys. B: Condens. Matter 404 (18) (2009) 2851–2853.
[37] A.F. Voter, S.P. Chen, High Temperature Ordered Intermetallic Alloys of Materials Research Society Symposium Proceedings Materials Research Society, Pittsburgh, Pennsylvania, 1987, p. 175.
[38] C.J. Smith, Metal Reference Book, 7th ed., Butterworth, London, 1976.
[39] W. Wycisk, M. Feller-Kniepmeier, J. Nucl. Mater. 69–70 (1978) 616.
[40] L.E. Murr, Interfacial Phenomena in Metals and Alloys, Addison-Wesley, Reading, MA, 1975.
[41] C. Kittel, Introduction to Solid State Physics, Wiley-Interscience, New York, 1986.
[42] G. Henkelman, H. Jónsson, J. Chem. Phys. 111 (15) (2002). Surfaces, Interfaces, and Materials.
[43] Kazuaki Toyoura, Yukinori Koyama, Akihide Kuwabara, Phys. Rev. B 78 (2008) 214303.
[44] N. Sandberg, B. Magyari-Kope, T.R. Mattsson, Phys. Rev. Lett. 89 (2002) 065901.
[45] C. Wert, C. Zener, Phys. Rev. 76 (8) (1949) 1169–1175.
[46] Chelsey L. Zacherl, www.ccmd.psu.edu/publications/theses/media/Zacherl, DissertationFinal.pdf.
[47] J.L. Bocquet, G. Brebec, Y. Limoge, Diffusion in Metals and Alloys, Elsevier Science BV, Amsterdam, The Netherlands, 1996. pp. 535.
[48] C.E. Campbell, A.L. Rukhin, Acta Mater. 59 (2011) 5194–5201.
[49] W. Gust, M.B. Hintz, A. Loddwg, H. Odelius, B. Predel, Phys. Stat. Sol. (a) 64 (1) (1981) 187–194.
[50] R.A. Swalin, A. Martin, J. Metals 8 (1956) 567.
[51] Tsuyoshi Yamamoto, Toshiyuki Takashima, Keizo Nishida, Trans. Jpn. Inst. Metals 21 (9) (1980) 601–608.
[52] A. Leenaers, C. Detavernier, S. Van den Berghe, J. Nucl. Mater. 381 (2008) 242–248.
[53] I.V. Belova, G.E. Murch, Philos. Mag. A 80 (7) (2000) 1469–1479.